Torque Ripple Minimization in Hybrid Stepper Motors Using Acceleration Measurements ⋆

Riccardo Antonello, Angelo Cenedese and Roberto Oboe

University of Padova, Department of Management and Engineering, Vicenza, Italy (Tel: +39-0444-998844; (e-mail: antonello@gest.unipd.it; angelo.cenedese@unipd.it; roberto.oboe@unipd.it)

Abstract: Hybrid stepper motors (HSMs) are commonly used in many cost-sensitive industrial and consumer applications. With the use of micro-stepping techniques, they could theoretically achieve a very high resolution in positioning of mechanical loads, even without position sensors. However, it is well known that HSMs are affected by a large torque ripple, due to cogging and phase unbalancing. This, in turn, may cause large vibrations on the load, especially in those systems with flexible elements (e.g. transmission belts). Several solutions have been proposed to alleviate this problem, but most of them make use of a load-side position sensor, by means of which it is possible to determine a position-dependent torque ripple profile, to be compensated during operations. Introducing a high resolution sensor on the load side, however, makes the cost of the system higher, thus vanishing the advantage of having a low cost open-loop actuator. Additionally, it is not always possible to accommodate a new position sensor on an existing mechanical system. In this paper, we propose a new system to compensate for the first two harmonics of the torque ripple in HSMs, based on the use of a load-side MEMS accelerometer, which can be easily fitted into existing systems, without any major modifications. The automated procedure developed minimizes the torque ripple by acting on the offset and amplitude of the phase currents. Experimental results on systems with and without load elasticity are reported, proving the effectiveness of the proposed approach.

Keywords: Hybrid stepper motor, MEMS accelerometers

1. INTRODUCTION

Stepper motors are commonly used in those motion control applications that do not require extremely high positioning accuracy, but instead impose constraints on cost and complexity of the driving circuits. Hybrid stepper motors (HSMs) are a particular kind of stepper motors operating under the combined principles of the permanent magnet (PM) and variable reluctance (VR) motors [Kenjo, 1984]. The structure of a hybrid stepper motor is depicted in Fig. 1. The rotor consists of a cylindrically shaped permanent magnet core magnetized along the cylinder axis, whose poles are covered by two laminated soft steel toothed end-caps. Teeth in the two end-caps are misaligned with respect to each other by half a tooth pitch. The stator has typically eight poles, and each pole has between two and six teeth. The stator tooth pitch is usually equal to the rotor tooth pitch, but in some motors is a little larger to improve the positioning accuracy and reduce the detent torque. In a bipolar two-phase hybrid stepper motor (as considered in Sec. 2), two windings (phases) are alternatively arranged on the stator poles to form coils through which the flow of the permanent magnet flux can be enhanced or reduced. Successive coils of each phase are wound in opposite sense, so that the same phase current generates oppositely oriented magnetic fields in opposite stator poles. Thanks to the skew arrangement of the rotor end-caps, the rotor moves in steps of a quarter of rotor tooth pitch when the two phases are excited with a conventional one-phase-on scheme (i.e. each phase is excited in turn with a positive or negative rated

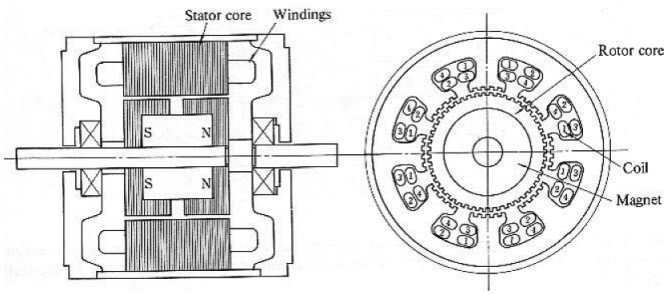

Fig. 1. Electromechanical structure of a hybrid stepper motor (after [Kenjo, 1984]).

⋆ This work has been partially supported by the Programma Operativo F.S.E. 2007-2013 Regione Veneto, Codice Progetto 2105/101/17/2214/2009 ("Modellizzazione Orientata al Controllo di Sistemi Meccatronici").

current): hence, a fine angular positioning resolution can be achieved with a sufficiently high number of rotor teeth. For example, in a motor with 50 rotor teeth (typical specification for several commercial products), the step length is 1.8°. Unfortunately, the generated torque is not smooth, being affected by undesired pulsations (harmonic components) that produce an irregular motion of the load. Non-smoothness of the generated torque becomes even more problematic in case of a resonant load, where the torque ripple could excite the load resonances, thus producing unacceptably large oscillations. Therefore, the reduction of torque ripple is highly desirable in many motion control applications.

The adoption of a sine-cosine microstepping excitation scheme, in which the two phases are excited with two sinusoidal quadrature currents, is perhaps the most conventional strategy used to alleviate (but not definitely remove) the torque ripple. Several other methods have been proposed in literature for reducing or compensating the torque ripple in permanent magnet synchronous motors - see [Jahns and Soong, 1996] and the references therein. However, the majority of the proposed methods requires a high resolution encoder for measuring the rotor angular position on the load side. This requirement is obviously counterintuitive in stepper motor applications, because of the intrinsic open-loop nature of the actuator.

In this paper, the problem of minimizing the torque ripple induced by uncalibrated offsets and amplitudes of the phase currents in a microstepping excitation scheme is considered. The proposed procedure is specifically conceived for finding the optimal offset and amplitude compensation values by relying only on the acceleration measurements provided by a low–cost MEMS accelerometer placed on the load side. Compared to other existing solutions, the one proposed in this paper has the advantage of being inexpensive and easily adaptable to existing systems. The paper is organized as follows. In Sec. 2 a model of the torque ripple generated by an HSM excited with a (unideal) microstepping scheme is presented; such model is then used in Sec. 3 to describe the proposed minimization procedure. The experimental results obtained with both an inertial and a resonant load are reported in Sec. 4. Finally, conclusions and future research directions are reported in Sec. 5.

2. HSM TORQUE RIPPLE

A bipolar two-phase permanent magnet (PM) hybrid stepper motor (HSM) is considered in the following. An analytical expression of the generated torque can be obtained by applying the principle of energy conservation; under the simplifying assumption that no magnetic saturation occurs in the magnetic circuit (i.e. the magnetic flux is proportional to the stator currents and independent of the internal magnet), it can be proved [Khorrami et al., 2003] that the motor torque τ_m, w.r.t. the rotor position θ, is equal to

$$\tau_m = \frac{1}{2}\boldsymbol{i}^T \frac{\partial \boldsymbol{L}}{\partial \theta}\boldsymbol{i} \tag{1}$$

where $\boldsymbol{L}$ is a 3×3 symmetric positive definite inductance matrix

$$\boldsymbol{L} = \begin{bmatrix} L_{11} & L_{12} & L_{1f} \\ L_{12} & L_{22} & L_{2f} \\ L_{1f} & L_{2f} & L_{ff} \end{bmatrix} \tag{2}$$

and $\boldsymbol{i} = [i_1, i_2, i_f]^T$, with i_1, i_2 the the winding currents in, respectively, phase 1 and phase 2, and i_f is the constant fictitious field current used to describe the magnetic field produced by the permanent magnet. In the inductance matrix, L_{11} and L_{22} are the self-inductances of windings 1 and 2, L_{12} is the mutual inductance between the two windings, L_{1f} and L_{2f} are the mutual inductances between the two windings and the fictitious rotor winding, and L_{ff} is the self-inductance of the fictitious rotor winding.

The torque expression (1) can be expanded as follows

$$\begin{aligned}\tau_m =& \tau_{pm} + \tau_{vr} + \tau_{cg} = \left(\frac{\partial L_{1f}}{\partial \theta} i_1 i_f + \frac{\partial L_{2f}}{\partial \theta} i_2 i_f\right) \\ &+ \left(\frac{1}{2}\frac{\partial L_{11}}{\partial \theta} i_1^2 + \frac{1}{2}\frac{\partial L_{22}}{\partial \theta} i_2^2 + \frac{\partial L_{12}}{\partial \theta} i_1 i_2\right) + \frac{1}{2}\frac{\partial L_{ff}}{\partial \theta} i_f^2\end{aligned} \tag{3}$$

The first term in round brackets is the torque component generated by the interaction of the magnetic fields produced by the stator windings and the permanent magnet. The second term is the *reluctance torque* and depends on the variations in self and mutual inductance of the windings (mainly due to geometric imperfections and rotor anisotropy). The last term is the *cogging* (or *detent*) *torque* and is mainly due to variations in self-inductance of the fictitious rotor winding caused by the presence of slots in the stator (minimum reluctance path). The cogging torque is present even in absence of winding currents; its periodicity with respect to the rotor position is equal to the periodicity at which the slots are located along the stator.

All the entries of the inductance matrix are periodic functions of the rotor position θ, and their basic frequencies can be deduced from the symmetries of the motor. Denoting with N_r the number of rotor teeth, it holds that

$$L_{11}(\theta) = L_0 + L_1 \cos(2N_r\theta) \tag{4}$$

$$L_{22}(\theta) = L_0 - L_1 \cos(2N_r\theta) \tag{5}$$

$$L_{12}(\theta) = -\frac{L_0}{2} + L_1 \sin(2N_r\theta) \tag{6}$$

$$L_{1f}(\theta) = L_{m0} + \sum_{j=1}^{n} L_{mj} \cos(jN_r\theta) \tag{7}$$

$$L_{2f}(\theta) = L_{m0} + \sum_{j=1}^{n} L_{mj} \sin(jN_r\theta) \tag{8}$$

$$L_{ff}(\theta) = L_{f0} + \sum_{j=4}^{n} L_{fj} \cos(jN_r\theta) \tag{9}$$

where n is the number of harmonics considered in the expression of the motor torque. Higher order harmonics ($n \geq 2$) in the mutual inductance terms L_{1f} and L_{2f} model the nonsinusoidal (with respect to the rotor angle) flux distribution in the airgap.

In a typical (ideal) hybrid stepper motor, the variation of phase inductance is as small as a few percent, and its contribution to the total torque is negligible; moreover, the surfaces of the rotor and stator teeth are shaped so that the magnetic flux in the airgap is almost sinusoidal.

By setting

$$L_{11} = L_{22} = L_0, \quad L_{12} = 0, \quad L_{mj} = 0 \quad j \geq 2 \tag{10}$$

in the self and mutual inductances (4)−(9), and replacing them in the torque components, (3) yields

$$\tau_{pm} = -i_1 i_f L_{m1} N_r \sin(N_r\theta) + i_2 i_f L_{m1} N_r \cos(N_r\theta) \quad (11)$$

$$\tau_{cg} = -\frac{1}{2}\sum_{j=4}^{n} L_{fj} j N_r \sin(jN_r\theta) i_f^2 \quad (12)$$

and $\tau_{vr} = 0$.

One way to generate an ideally constant torque consists of adopting a microstepping driving technique, in which two sinusoidal quadrature currents are imposed into the stator windings:

$$i_1 = I\cos(N_r\theta_u)\,, \qquad i_2 = I\sin(N_r\theta_u) \quad (13)$$

where θ_u is the angular position of the stator flux. In fact, replacing (13) in (11) yields:

$$\tau_{pm} = i_f L_{m1} N_r\, I\, \sin\left[N_r(\theta_u - \theta)\right]. \quad (14)$$

Hence, the torque τ_{pm} is constant whenever the angle $\rho = \theta_u - \theta$, called *torque* (or *load*) *angle*, is constant.

In practice, due to unbalancing and imperfections of the driving amplifiers, the phase currents will always be affected by some offset, and their amplitude will be unmatched. By taking into account the offsets and gain unbalancing in the expressions of phase currents, i.e.

$$i_1 = I_{10} + I_{11}\cos(N_r\theta_u)\,, \quad i_2 = I_{20} + I_{21}\sin(N_r\theta_u) \quad (15)$$

and replacing them in (11) yields:

$$\begin{aligned}\tau_{pm} = i_f L_{m1} N_r \Big\{ & \frac{1}{2}(I_{11}+I_{21})\sin[N_r(\theta_u-\theta)] \\ & - I_{10}\sin(N_r\theta) + I_{20}\cos(N_r\theta) \\ & - \frac{1}{2}(I_{11}-I_{21})\sin[N_r(\theta+\theta_u)] \Big\}\end{aligned} \quad (16)$$

For a constant torque angle $\rho = \theta_u - \theta$, two harmonic components show up in the torque τ_{pm}, in addition to a constant term. The first harmonic component of the torque ripple in τ_{pm} has the same frequency of the phase currents and an amplitude depending on the current offsets I_{10} and I_{20}; the second component has twice the frequency of the phase currents and an amplitude depending on the unbalancing of the phase current amplitudes I_{11} and I_{21}.

3. TORQUE RIPPLE MINIMIZATION IN HSMS

Several methods have been proposed in literature for reducing or compensating the torque ripple in permanent magnet synchronous motors; a rather complete review is reported in [Jahns and Soong, 1996]. The methods can be broadly classified in two major categories: 1) methods based on the improvement of the machine design and the torque generation mechanism, and 2) methods based on the improvement of the excitation scheme, possibly exploiting open or closed control loop schemes for compensating the nonideal characteristics of the machine.

A well known design expedient to reduce the torque ripple in hybrid stepper motors consists of skewing the two endcaps of the rotor by half the rotor tooth pitch. A review of many classical and innovative design techniques for smooth torque generation in PM motors are reported in [Bianchi and Bolognani, 2002].

Regarding the second category of torque ripple minimization methods, the most typical example is perhaps the so-called sine-cosine microstepping excitation scheme, in which two sinusoidal quadrature currents are imposed to the stator windings. With such method, the magnetic flux generated by the stator rotates smoothly, thus reducing torque ripple and rotor oscillations. Nevertheless, the residual torque ripple could be still too large, especially in presence of large cogging torque. In order to further reduce the torque ripple, a broad range of alternative techniques, based either on feedforward or feedback compensation schemes, have been proposed so far in literature.

The usual feedforward compensation scheme consists of using programmed excitation waveforms for the phase currents to cancel the pulsating torque components. In the majority of the cases, the phase current profiles are shaped by injecting suitable harmonic components that selectively eliminate the torque ripple components, similarly to what originally proposed in [Le-Huy et al., 1986]. In [Favre et al., 1993], the compensating harmonics are determined by employing an iterative procedure; in [Hung and Ding, 1993], [Hanselman, 1994] and, more recently [Wu and Chapman, 2005], the current profiles for eliminating the torque ripple components up to a given harmonic order are computed in closed form by employing numerical optimization techniques, once the back emf waveforms are known. In [Ferretti et al., 1998], a compact model for the pulsating torque in PM motors is used to perform a feedforward compensation on the position controller output; the unknown parameters of the model are identified by performing simple closed-loop motion experiments. More advanced compensation schemes exploit adaptive [Chen and Paden, 1993] or nonlinear [Taylor, 1994], [Bodson et al., 1993] feedback control techniques to generate smoother torques. In any case, all the aforementioned solutions share the common drawback of requiring the measurement of the rotor position: this is a rather restrictive assumption for stepper motor applications, where the actuator is specifically chosen to perform accurate positioning in open-loop, without requiring any load-side position sensor (e.g. a high resolution encoder).

3.1 Proposed scheme

Differently from most of the solutions available in literature, the procedure for torque ripple reduction proposed in this paper does not require any expensive high-resolution encoder for measuring the rotor angular position; instead, it makes use of a low-cost MEMS accelerometer to detect the vibration induced by the torque ripple on the load-side. Apart from cost considerations, another advantage of the proposed solution is that it can be easily fitted in existing equipments, without requiring substantial interventions.

The proposed procedure is conceived to minimize the torque ripple contribution induced by imperfections in the generation of the current profiles when using a microstepping excitation scheme. As already mentioned in Sec. 2, two imperfections are considered, namely undesired nonzero offsets in phase currents and unbalanced gains in the driving amplifiers of the two phases. The compensation scheme is based on the observation that, under the assumption made in Sec. 2, the nonzero current offsets produce a torque harmonic disturbance component at the same frequency of the driving currents, while the

amplitude unbalancing between the two current phases generates a second harmonic at twice the frequency of the driving currents.

With reference to (16), it can be noted that the two torque ripple harmonics have magnitudes

$$|\tau_{pm,1}| = i_f L_{m1} N_r \sqrt{I_{10}^2 + I_{20}^2} \quad (17)$$

$$|\tau_{pm,2}| = i_f L_{m1} N_r \frac{1}{4} |I_{11} - I_{21}| \quad (18)$$

i.e. the squared magnitude of the first harmonic depends quadratically on the current offsets I_{10} and I_{20}, while the squared magnitude of the second harmonic depends quadratically on the amplitude unbalancing $I_{11} - I_{21}$. This observation allows to formulate a multi-step minimization procedure, in which some current offsets and gain unbalancing are deliberately introduced in the phase currents, and then varied to seek for a minimum of the amplitude of the first two harmonics of the acceleration ripple measured by the MEMS accelerometer.

The procedure can be summarized in the following steps:

(1) do a first experiment in which the ideal microstepping excitation scheme (15) is modified as follows

$$i_1 = \hat{I}_{10} + I\cos(N_r\theta_u)\,, \quad i_2 = I\sin(N_r\theta_u) \quad (19)$$

where the offset $\hat{I}_{10}$ is slowly varied over a specified range (fraction of the rated current I), while the rotor moves with almost constant velocity (i.e. while θ_u is slowly linearly increased).
By using a conventional synchronous amplitude demodulation scheme, extract the amplitude of the first harmonic of the acceleration ripple measured by the MEMS accelerometer.
Then, use the (weighted) least squares method to fit a parabola to the data consisting of the squared magnitude of the first harmonic vs. the values of the offset $\hat{I}_{10}$: the minimum of the parabolic fit gives the optimal offset compensation value $\hat{I}_{10}^*$ for the phase current i_1.

(2) do a second experiment in which the previous step is repeated for the second phase current. Use the modified microstepping excitation scheme

$$i_1 = \hat{I}_{10}^* + I\cos(N_r\theta_u)\,,\ i_2 = \hat{I}_{20} + I\sin(N_r\theta_u) \quad (20)$$

where the offset $\hat{I}_{20}$ is slowly varied over a specified range. Obtain the optimal offset compensation value $\hat{I}_{20}^*$ by repeating the procedure described in the previous step.

(3) do a third experiment in which the ideal microstepping excitation scheme (15) is modified as follows

$$i_1 = \hat{I}_{10}^* + \hat{I}_{11}\cos(N_r\theta_u) \quad (21)$$

$$i_2 = \hat{I}_{20}^* + \hat{I}_{21}\sin(N_r\theta_u) \quad (22)$$

where $\hat{I}_{11}$ is slowly varied over a specified range (across the rated current I), while $\hat{I}_{21} = 2\,I - \hat{I}_{11}$. The last condition guarantees that the average torque provided to the load during the whole experiment is kept constant, despite the unbalancing of the phase current amplitudes - see equation (16).
By using a conventional synchronous amplitude demodulation scheme, extract the amplitude of the second harmonic of the acceleration ripple measured by the MEMS accelerometer.
Then, use the (weighted) least squares method to fit a parabola to the data consisting of the squared magnitude of the second harmonic vs. the values of the current amplitude $\hat{I}_{11}$: the minimum of the parabolic fit gives the optimal amplitude value $\hat{I}_{11}^*$ for the phase current i_1 (and, indirectly, the optimal amplitude value $\hat{I}_{21}^*$ for the phase current i_2).

In principle, the three steps described above can be iterated many times to refine the estimation of the optimal compensation values; however, it has been noted that a single iteration is generally sufficient for attaining the optimal values with a satisfactory accuracy level.

4. EXPERIMENTAL RESULTS

The proposed procedure for minimizing the torque ripple in hybrid stepper motors has been tested on a commercial bipolar, two-phase HSM with 1.8° step angle (50 rotor teeth) driving either an inertial or a resonant load. The inertial load has been chosen as a steel disk with relatively small inertia, mounted directly on the motor shaft; as for the resonant load, an elastic transmission system based on a pair of reduction gears (reduction ratio $N_G = 1/7$) connected by a toothed belt has been considered (see Fig.2). Such transmission system is part of the mechanism used for generating the pan and tilt motions in a positioning unit for surveillance cameras (see Fig.3).

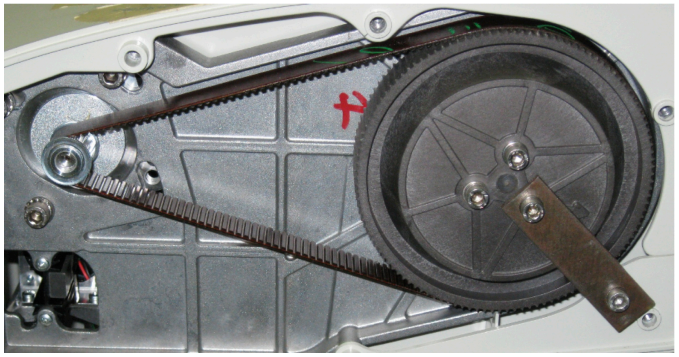

Fig. 2. Elastic transmission system composed of reduction gears and a toothed belt.

Since the experimental results are similar for the inertial and the resonant loads, only the latter are discussed in the remaining part of this section, due to space constraints.

The proposed procedure has been applied to reduce the vibration induced by the motor torque ripple on the pan motion of the positioning unit. Therefore, a MEMS linear accelerometer has been placed on top of the camera, as shown in Fig. 4, to measure the tangential acceleration of the unit; then, the angular acceleration can be derived by measuring the distance of the accelerometer from the rotation axis.

Two sinusoidal phase currents with a nominal amplitude of $I = 1\,A$ and a frequency of $20\,Hz$ (corresponding to an angular velocity of $\approx 21°/s$ for the pan motion)

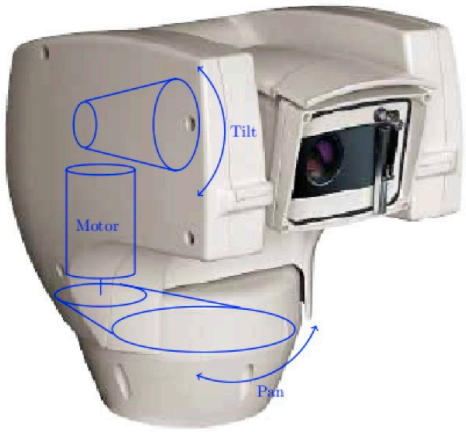

Fig. 3. Positioning unit for surveillance cameras.

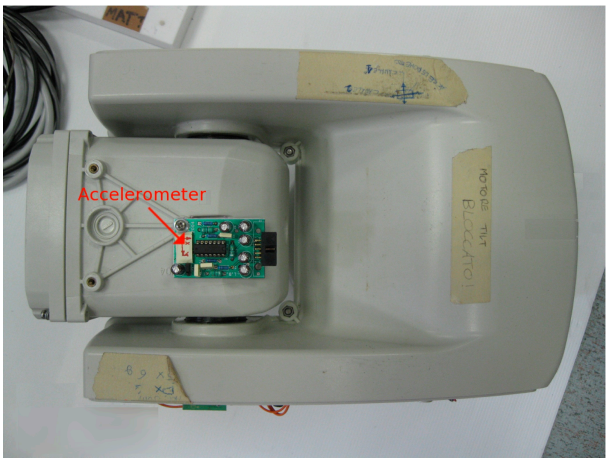

Fig. 4. MEMS accelerometer placement on top of the camera case.

have been used in the experiments. The driving frequency has been selected to avoid the excitation of the load resonances, thus generating a more regular motion in which the acceleration variations produced by varying the current offsets/amplitudes can be highlighted more clearly. Due to an inaccurate initial calibration of the offsets and gains of the linear amplifiers used to drive the two motor phases, the phase currents are affected by some offset and gain unbalancing, as shown in the top plot of Fig. 5.

The application of the procedure described in the previous section yields the results collectively reported in Fig. 6. The two current offsets have been varied in the range $-0.5\,A \div 0.5\,A$ (corresponding to $\pm 50\%$ of the nominal rated current $I = 1\,A$); the minimization of the first harmonic amplitude has been achieved with the offset values $\hat{I}^*_{10} = -0.121\,A$ and $\hat{I}^*_{20} = -0.055\,A$ (see the top plots of Fig. 6). The phase current amplitudes have been unbalanced up to 30 % of the nominal rated current (i.e. the amplitude of one phase current has been varied in the range $0.7\,A \div 1.3\,A$, while the remaining one has been adjusted to keep the sum constant to $2\,I = 2\,A$). The minimization of the second harmonic amplitude is obtained with the amplitude values $\hat{I}^*_{11} = 0.847\,A$ and $\hat{I}^*_{21} = 2\,I - \hat{I}^*_{11} = 1.153\,A$.

It is worth noticing that the measured square magnitudes of the first two acceleration harmonics depend quadratically on the two current offsets and the amplitude unbalancing, thus legitimating the assumptions made in Sec. 2 for deriving the torque expression (16). However, differently from what could be argued by using (17) and (18), the measurements of the compensated currents reported in the bottom plot of Fig. 6 show that the torque ripple minimization is attained with some residual small offsets and gain unbalancing.

This discrepancy between the predicted and experimental results is explained by the inductance terms neglected in the derivation of (16), especially those describing the nonsinusoidal flux distribution in the airgap (higher order harmonics in the mutual inductance terms L_{1f} and L_{2f}).

The benefits of the proposed compensation procedure in minimizing the first two harmonics of the torque ripple

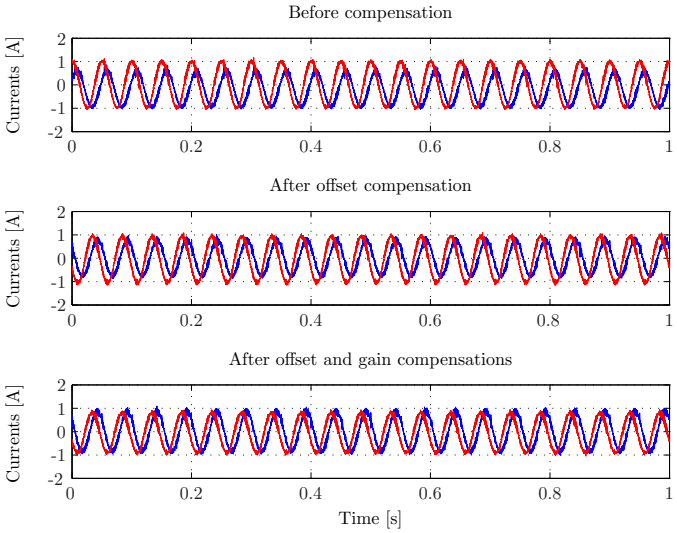

Fig. 5. Phase currents measurements before and after the compensation procedure.

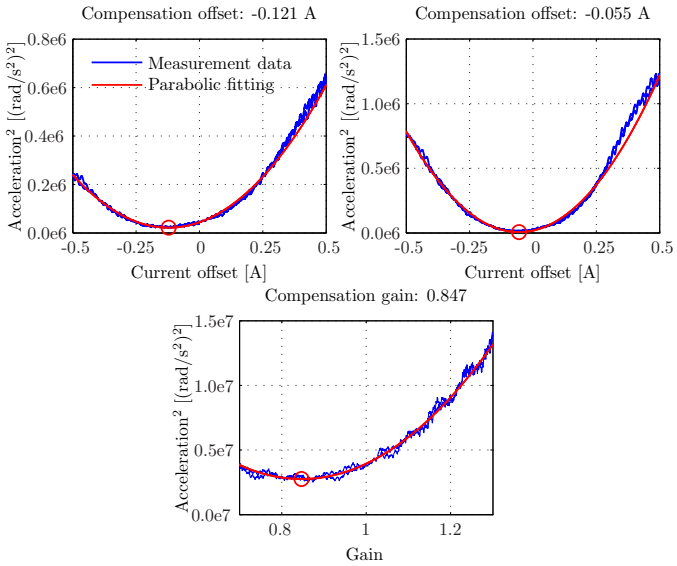

Fig. 6. Determination of the optimal phase current offsets (top plots) and amplitude unbalancing (bottom plot).

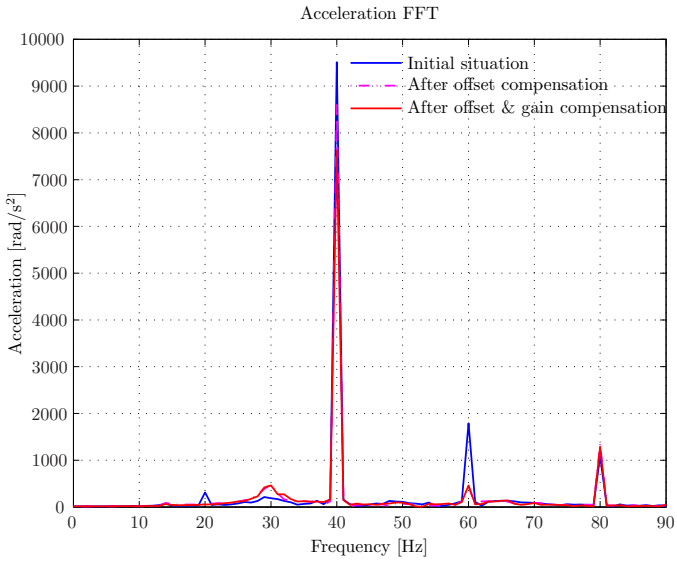

Fig. 7. Acceleration ripple (load-side) spectrum before and after the compensation procedure.

can be also appreciated in the acceleration spectrum measurements reported in Fig. 7. The compensation of the current offsets drastically reduces the amplitude of the first harmonic (at $20\,Hz$); the minimization of the second harmonic amplitude is less evident (at $40\,Hz$), perhaps due to the fact that the initial gains of the driving amplifiers were almost balanced before applying the compensation procedure.

5. CONCLUSIONS

This paper has presented a procedure for minimizing the torque ripple induced in HSMs by uncalibrated offsets and amplitudes of the phase currents generated with a microstepping driver. The proposed method relies exclusively on the acceleration measurement provided by a low–cost MEMS accelerometer placed on the load–side: no high-resolution, expensive encoders are needed for measuring the rotor position, as usually required in many compensation schemes available in literature. The effectiveness of the proposed solution has been experimentally proved, in both the cases of an inertial and a resonant load.

Some (experimentally validated) working assumptions have been considered for the definition of the compensation procedure: in particular, the effects of the reluctance torque and the nonsinusoidal flux distribution in the air-gaps have been almost neglected.

A future development of the present work consists of understanding how the neglected terms (such as the reluctance torque and high order harmonic components in the cogging torque) affect the torque ripple, and how they can be effectively included in the minimization procedure.

6. ACKNOWLEDGEMENTS

The authors would like to thank Videotec (Schio, Vicenza, Italy) for providing (and allow us to hack) the camera positioning units, and Andrea Parisotto, Daniele Pellizzer, Marco Peruzzo and Mattia Schiesaro for their valuable contribution to the experimental activity.

REFERENCES

N. Bianchi and S. Bolognani. Design techniques for reducing the cogging torque in surface-mounted PM motors. *Industry Applications, IEEE Transactions on*, 38(5):1259 – 1265, sep. 2002. ISSN 0093-9994. doi: 10.1109/TIA.2002.802989.

M. Bodson, J.N. Chiasson, R.T. Novotnak, and R.B. Rekowski. High-performance nonlinear feedback control of a permanent magnet stepper motor. *Control Systems Technology, IEEE Transactions on*, 1(1):5 –14, mar. 1993.

D. Chen and B. Paden. Adaptive linearization of hybrid step motors: stability analysis. *Automatic Control, IEEE Transactions on*, 38(6):874 –887, jun. 1993. ISSN 0018-9286. doi: 10.1109/9.222300.

E. Favre, L. Cardoletti, and M. Jufer. Permanent-magnet synchronous motors: a comprehensive approach to cogging torque suppression. *Industry Applications, IEEE Transactions on*, 29(6):1141 –1149, nov. 1993. ISSN 0093-9994. doi: 10.1109/28.259725.

G. Ferretti, G. Magnani, and P. Rocco. Modeling, identification, and compensation of pulsating torque in permanent magnet AC motors. *Industrial Electronics, IEEE Transactions on*, 45(6):912 –920, dec. 1998. ISSN 0278-0046. doi: 10.1109/41.735335.

D.C. Hanselman. Minimum torque ripple, maximum efficiency excitation of brushless permanent magnet motors. *Industrial Electronics, IEEE Transactions on*, 41(3):292 –300, jun. 1994. ISSN 0278-0046. doi: 10.1109/41.293899.

J.Y. Hung and Z. Ding. Design of currents to reduce torque ripple in brushless permanent magnet motors. *Electric Power Applications, IEE Proceedings B*, 140(4):260 – 266, jul. 1993. ISSN 0143-7038.

T.M. Jahns and W.L. Soong. Pulsating torque minimization techniques for permanent magnet AC motor drives-a review. *Industrial Electronics, IEEE Transactions on*, 43(2):321 –330, apr. 1996. ISSN 0278-0046. doi: 10.1109/41.491356.

T. Kenjo. *Stepping Motors and Their Microprocessor Controls*. Clarendon Press, Oxford, 1984.

F. Khorrami, P. Krishnamurthy, and H. Melkote. *Modeling and adaptive nonlinear control of electric motors*. Springer-Verlag, Berlin, 2003.

Hoang Le-Huy, Robert Perret, and Rene Feuillet. Minimization of Torque Ripple in Brushless DC Motor Drives. *Industry Applications, IEEE Transactions on*, IA-22(4):748 –755, jul. 1986. ISSN 0093-9994. doi: 10.1109/TIA.1986.4504787.

D.G. Taylor. Nonlinear control of electric machines: an overview. *Control Systems Magazine, IEEE*, 14(6):41 – 51, dec. 1994. ISSN 0272-1708. doi: 10.1109/37.334414.

A.P. Wu and P.L. Chapman. Simple expressions for optimal current waveforms for permanent-magnet synchronous machine drives. *Energy Conversion, IEEE Transactions on*, 20(1):151 – 157, mar. 2005. ISSN 0885-8969. doi: 10.1109/TEC.2004.837299.